Poincaré index formula, vortices and superflow saddle points in a non-rotating cold atom Bose-Einstein condensate

Julien Garaud[1, 2, *] and Antti J. Niemi[1, 2, 3, 4, †]

[1] *Nordita, Stockholm University, Roslagstullsbacken 23, SE-106 91 Stockholm, Sweden*
[2] *Institut Denis Poisson CNRS-UMR 7013, Université de Tours, 37200 France*
[3] *Pacific Quantum Center, Far Eastern Federal University, 690950 Sukhanova 8, Vladivostok, Russia*
[4] *Department of Physics, Beijing Institute of Technology, Haidian District, Beijing 100081, China*

(Dated: August 9, 2021)

A dilute gas of Bose-Einstein condensed atoms, in a non-rotating and axially symmetric harmonic trap, can be modelled by the time dependent Gross-Pitaevskii equation. The minimum energy solutions describe vortices that propagate around the trap center. The number of vortices increases with increasing angular momentum, and the vortices repel each other to form Abrikosov lattices. Besides vortices there are also saddle points, where the velocities of the superflow of distinct vortices cancel each other. The Poincaré index formula states that the difference in the number vortices and saddles points can never change. When the number of saddle points is small, they aggregate and form degenerate propagating structures. However, when their number becomes sufficiently large there is a transition and the saddle points start dispersing. They pair up with vortices and propagate around the trap center in regular arrangements akin Abrikosov lattices.

I. INTRODUCTION

Topological invariants that characterize a physical system are enticing, as they often describe properties of the system that remain unchanged under its continuous deformations. As a consequence, topology is widely used to identify and portray robust physical phenomena; topological techniques are now commonplace in numerous applications from fundamental interactions to condensed matter, fluid dynamics and beyond [1]. Here we extend the repertoire of topological techniques that can be used to analyze the properties of vortices in a cold atom Bose-Einstein condensate. This condensate is a coherent macroscopic quantum state, with unique features that facilitate a high level of experimental control [2–4].

Bose-Einstein condensates that are formed in a trapped gas of ultra-cold alkali atoms are studied extensively, both in earth-bound and in earth-orbiting laboratory experiments [5]. Among the emerging applications is the development of ultra-sensitive sensors and detectors [6]. The properties of cold atom condensates are also under active investigation, as a potential platform for quantum computation and simulation [7].

In a theoretical approach, a Bose-Einstein condensate of cold atoms is commonly modeled by a macroscopic, complex-valued wave function $\psi(\mathbf{x}, t)$. The modulus $|\psi(\mathbf{x}, t)|$ of the wave function describes the density of the condensate and its phase determines the velocity vector field of the superflow

$$\mathbf{v}(\mathbf{x}, t) = \boldsymbol{\nabla} \arg[\psi](\mathbf{x}, t)\,. \tag{1}$$

The principal topological excitations in these condensates are vortices [8]. In a two dimensional model, the core of a vortex is the point where the modulus of the wave function vanishes, and is a also center of the superflow velocity $\mathbf{v}(\mathbf{x}, t)$. As a topological invariant, a vortex is commonly characterized by an integer valued circulation of the superflow velocity around its core.

In addition of vortex cores, there are also other fixed points that can characterize the two dimensional vector field $\mathbf{v}(\mathbf{x}, t)$. In particular, there can be saddle points where the velocity (1) of distinct vortices exactly cancel each other, while the density of the condensate does not vanish. The balance between the number of centers and the number of saddle points is a topological invariant that is governed by an index theorem.

From the knowledge of all its fixed points, a phase portrait of the vector field $\mathbf{v}(\mathbf{x}, t)$ can be constructed. The phase portrait characterizes the entire vector field $\mathbf{v}(\mathbf{x}, t)$ in a manner that is invariant under continuous local deformations. A phase portrait commonly describes adequately the solutions of the underlying dynamical equation, often without any need to actually solve the equation.

We first introduce the Poincaré index theorem that is relevant to describe the topological properties of the velocity of superflow in two space dimensions. We then apply the index theorem to characterize the solutions of the Gross-Pitaevskii equation that models a dilute, non-rotating condensate of cold atoms in an harmonic trap.

II. THEORETICAL FRAMEWORK

A. Poincaré index formula

As a two dimensional vector field, here the velocity of the superflow (1), supports an integer valued index

$$i_{\mathbf{v}}(p;\Gamma) = \frac{1}{2\pi}\oint_{\Gamma} d\boldsymbol{\ell}\cdot\mathbf{v} \equiv \frac{1}{2\pi}\oint_{\Gamma}\frac{v_x dv_y - v_y dv_x}{v_x^2+v_y^2} \in \mathbb{Z}\,. \tag{2}$$

Here Γ is a closed curve on the (x, y)-plane that does not pass through any fixed point of $\mathbf{v}(\mathbf{x})$. The index is a

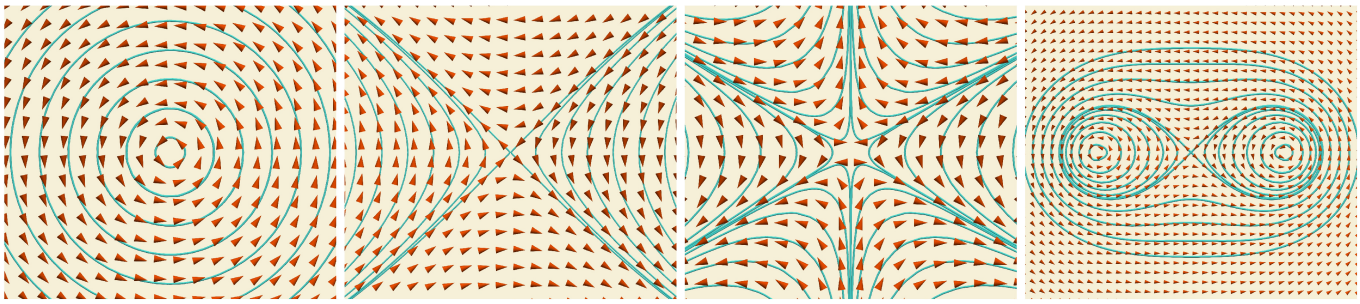

Figure 1. Phase portraits that are encountered in the present study of the superflow velocity vector $\mathbf{v}(\mathbf{x})$ in (1). The red arrows show the vector field $\mathbf{v}(\mathbf{x})$, and the cyan lines represent its streamlines. The leftmost panel shows a center that corresponds to a single vortex with $i_{\mathbf{v}} = 1$. The two panels in the middle display saddle points with $i_{\mathbf{v}} = -1$ and $i_{\mathbf{v}} = -2$, respectively. The rightmost panel shows how a saddle point can appear in a phase portrait of two vortices (centers). It is a point where the velocities of the superflows of the two distinct vortices cancel each other.

topological invariant, which computes the quantized circulation of the vector field $\mathbf{v}(\mathbf{x})$. A single isolated vortex core p is a fixed point, *i.e.* a *center*, of $\mathbf{v}(\mathbf{x})$. For a closed curve that encircles once a single vortex core p in the counterclockwise direction, the index is $i_{\mathbf{v}}(p;\Gamma) = +1$.

Centers are not the sole fixed points of the vector field $\mathbf{v}(\mathbf{x})$. But all the fixed points can be detected by the Poincaré index formula, and a phase portrait of the vector field $\mathbf{v}(\mathbf{x})$ can then be constructed: The Poincaré index formula states that for any (sufficiently regular) closed curve Γ that encloses finitely many fixed points $p_1, p_2, ...p_k$ of $\mathbf{v}(\mathbf{x})$, the sum of their indexes (2) obeys [9, 10]

$$\text{Index} \;=\; \sum_{j=1}^{k} i_{\mathbf{v}}(p_j;\Gamma) = \mathcal{X}_\Gamma + \frac{1}{2}\left(I_\Gamma - E_\Gamma\right) . \qquad (3)$$

Here $\mathcal{X}_\Gamma$ is the Euler character of the area that is bounded by the curve Γ, with I_Γ the number of (concave) curve segments with tangencies that are internal to the area that is bounded by Γ, and E_Γ the number of (convex) curve segments where the tangencies are external to Γ.

We note that in the special case when the vector field points either outward or inward at a boundary trajectory of a region so that both I_Γ and E_Γ are absent, (3) reduces to the Poincaré-Hopf index theorem [11].

Another vector field, that depends on the modulus of the complex wave function $\psi(\mathbf{x}, t)$, can also be introduced as

$$\mathbf{w}(\mathbf{x}, t) = \boldsymbol{\nabla}|\psi(\mathbf{x}, t)| . \qquad (4)$$

Unlike the phase, the modulus of the wave function is a smooth and single valued, strictly non-negative function that vanishes at $\mathbf{x} \to \infty$ and at vortex cores. For any circular trajectory around the origin, with a sufficiently large radius so that it encircles all the vortex structures, the vector field (4) always points towards the interior so that the Poincaré-Hopf index formula applies; the index (2) has value $i_{\mathbf{w}} = +1$ and the large scale structure of the vector field (4) is that of a sink. A single vortex core is an isolated minimum value critical point of $|\psi(\mathbf{x}, t)|$, thus it is a source of (4) with index $i_{\mathbf{w}} = +1$. As a consequence the number of vortex cores is always balanced by accompanying saddle points, but for certain vortex configurations there are also degeneracies. This is the case *e.g.* when a single vortex is located at the center of the trap, the vortex core is encircled by a nodal line where the modulus $|\psi(\mathbf{x}, t)|$ has its maximum value, and the vector field (4) has a degeneracy circle. Instead of (2) the appropriate index theoretic analysis is then based on the degeneracy index introduced in [12].

B. Gross-Pitaevskii equation

We consider a two-dimensional Bose-Einstein condensate of N alkali atoms in an axially symmetric, non-rotating, harmonic trap $V(\mathbf{x}) = |\mathbf{x}|^2/2$. This approximates for example an anisotropic three dimensional trap, resulting in an oblate, essentially two dimensional spheroid condensate $\mathcal{D}$. The atoms interact with each other via a repulsive short range pair potential, so that in the limit where the number of atoms N becomes large, the condensate can be modeled by a solution of the time-dependent two dimensional Gross-Pitaevskii equation. This is a nonlinear Schrödinger equation for the complex valued wave function $\psi(\mathbf{x}, t)$ that describes the condensate as a coherent macroscopic quantum state.

With an appropriate choice of various scales and parameters, the relevant two dimensional time dependent Gross-Pitaevskii equation reads as follows [13]:

$$i\partial_t\psi = -\frac{1}{2}\boldsymbol{\nabla}^2\psi + \frac{|\mathbf{x}|^2}{2}\psi + g|\psi|^2\psi \equiv \frac{\delta F}{\delta\psi^\star} . \qquad (5)$$

The dimensionless coupling g specifies the strength of the pairwise interatomic interactions. In a typical experiment with 10^4–10^6 atoms its numerical values are $g \sim 10^1$–10^3. For a detailed discussion of the conventions used here, see [14].

We are interested in the ground state solution of (5)

that minimizes the Gross-Pitaveskii free energy

$$F = \int d^2x \left\{ \frac{1}{2}|\boldsymbol{\nabla}\psi|^2 + \frac{|\mathbf{x}|^2}{2}|\psi|^2 + \frac{g}{2}|\psi|^4 \right\} . \quad (6)$$

Since F is a strictly convex functional, its only critical point is the absolute minimum $\psi(\mathbf{x}) \equiv 0$. It follows that the ground state solution of the Gross-Pitaevskii equation can be timecrystalline [15] provided there are conserved quantities [16]: Besides the free energy F the time evolution (5) conserves two additional quantities, as Noether charges. One of these is

$$< \hat{\mathrm{N}} > \equiv \int d^2x\, \psi^\star \psi \;\equiv\; N = 1\,, \quad (7)$$

that counts the number of atoms. For clarity we have chosen the parameter values in (5), (6) so that the numerical value (7) is normalized to $N = 1$. For an axially symmetric trap, the macroscopic angular momentum along the z-axis

$$< \hat{\mathrm{L}}_z > \equiv \int d^2x\, \psi^\star(-i\boldsymbol{e}_z \cdot \mathbf{x} \wedge \boldsymbol{\nabla})\psi \;\equiv\; L_z = l_z\,, \quad (8)$$

is also conserved. The numerical value l_z of the canonical angular momentum of the condensate

$$\hat{\mathrm{L}}_z = -i\boldsymbol{e}_z \cdot \mathbf{x} \wedge \boldsymbol{\nabla} \equiv -i\partial_\theta\,, \quad (9)$$

with θ the polar angle around the z-axis, is a free parameter that can take an arbitrary value; see [14].

The *r.h.s.* of (5) can not vanish unless $\psi \equiv 0$, so that for non-vanishing values of the Noether charges, the minimum of F can not be a critical point of F. Thus, to construct the ground state wave function of (5), we use methods of constrained optimization and minimize the free energy (6) at the *fixed* values of the Noether charges (7) and (8). The Lagrange multiplier theorem [17] states that the minimum of (6) can be found as a critical point of

$$F_\lambda = F + \lambda_N(N-1) + \lambda_z(L_z - l_z)\,, \quad (10)$$

where the Lagrange multipliers λ_N, λ_z respectively enforce the values $N = 1$ and $L_z = l_z$ of the Noether charges. The critical points of F_λ obey

$$-\frac{1}{2}\nabla^2\psi + \frac{|\mathbf{x}|^2}{2}\psi + g|\psi|^2\psi = -\lambda_N\psi + \lambda_z(i\boldsymbol{e}_z \cdot \mathbf{x} \wedge \boldsymbol{\nabla})\psi, \quad (11)$$

together with the two conditions (7) and (8). From these three equations we solve for the critical point wave function $\psi_{cr}(\mathbf{x})$ and for the ensuing Lagrange multiplier values $\lambda_N^{cr}, \lambda_z^{cr}$. Note that both Lagrange multipliers are time independent [16], and that they cannot vanish simultaneously.

We focus on the critical points of (10) that are also minima of the free energy (6). Let $\{\psi_{min}(\mathbf{x}), \lambda_N^{min}, \lambda_z^{min}\}$ denote such a configuration. If $\psi_{min}(\mathbf{x})$ is an initial value of the Gross-Pitaevskii equation (5), then it obeys the *linear* time evolution

$$i\partial_t\psi = -\lambda_N^{min}\psi + i\lambda_z^{min}\boldsymbol{e}_z \cdot \mathbf{x} \wedge \boldsymbol{\nabla}\psi\,. \quad (12)$$

We recall (9), denote $\sigma = \lambda_N^{min}/\lambda_z^{min}$, and define

$$A_\theta = \mathbf{e}_z \cdot \mathbf{x} \wedge \boldsymbol{\nabla} \tan^{-1}(x/y)$$

This is a vector field on the plane with a center at the origin (x, y)=(0,0). The Poincaré index (2) is $i_{\mathbf{A}} = +1$ for any trajectory that encircles the origin once in counterclockwise direction; we note that A_θ is akin the azimuthal component of the vector potential of a line vortex along the z-axis. The time evolution (12) can further be written as

$$i\partial_t\psi = -\lambda_z^{min}(\hat{\mathrm{L}}_z + \sigma\, A_\theta)\psi \;\equiv\; -\lambda_z^{min}\,\hat{\mathrm{L}}_z^{\,cov}\psi\,. \quad (13)$$

In the presence of A_θ the rotations around the z-axis *i.e.* changes in the polar angle θ are generated by the covariant angular momentum operator $\hat{\mathrm{L}}_z^{\,cov}$ instead of the canonical (9). Thus the equation (12) describes the rotation of the initial wave function $\psi_{min}(\mathbf{x})$ around the center of the trap, with angular velocity λ_z^{min}.

In the following we are interested in the consequences of the Poincaré index formula (2), in the case of a vector field $\mathbf{v}(\mathbf{x}, t)$ that describes the velocity of the superflow (1) of the minimal energy solution of the Gross-Pitaevskii equation (5)) with initial condition $\psi(\mathbf{x}, t = 0) = \psi_{min}(\mathbf{x})$. We focus on the topological and geometrical properties of its fixed point structure, as the value of the angular momentum l_z is changed. For this we analyze the profile of the superflow vector field, by employing the index formula in combination with various different trajectories Γ.

III. NUMERICAL RESULTS

We have numerically constructed the critical points of (10) that minimize the Gross-Pitaevskii free energy (6), for $l_z > 0$ and with $g = 5$, 100 and 400. The problem is discretized within a finite-element framework [18], and the constrained optimization problem is solved using the Augmented Lagrangian Method (numerical methods are discussed in details in [14]). Whenever $l_z \neq 0$ the minimum free energy solution is a configuration with vortices and saddle points. Its time-evolution (5), (12) is also timecrystalline, as it always depends on the time variable t in a nontrivial fashion [14].

The number of vortices increases with l_z. Each new vortex enters the condensate at the boundary of the disk $\mathcal{D}$, and moves towards the trap center as l_z increases. Since the Euler character of a disk is $\mathcal{X}_\Gamma = 1$, the Poincaré index theorem ensures that, on the entire trapping disk $\mathcal{D}$, there is always one more vortex (center) than there are saddle points. That is, when the closed curve Γ coincides with the perimeter of the entire disk $\mathcal{D}$ in counterclockwise direction, the index (3) always has the value $i_{\mathbf{v}} = 1$.

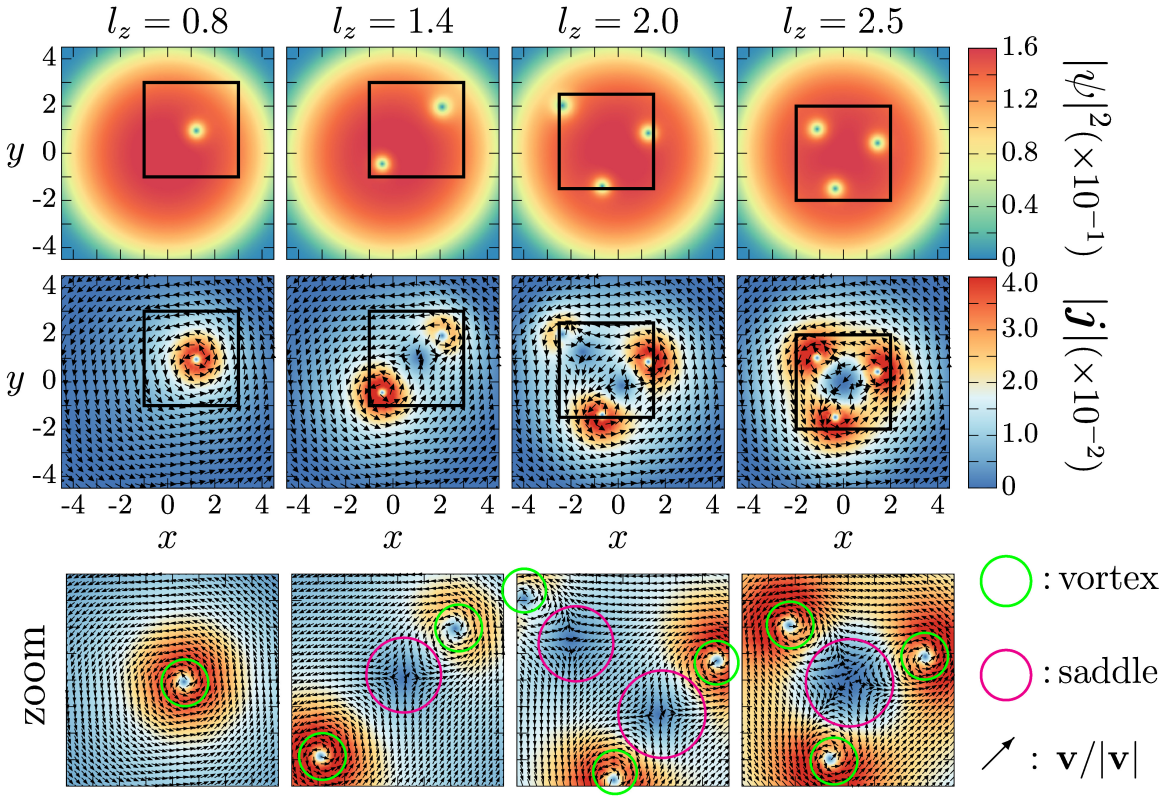

Figure 2. The panels on the different columns show examples of the minimal energy configurations of (6), that satisfy $L_z = l_z$ and $N = 1$ for the dimensionless coupling $g = 400$. The panels on the top row show the density $|\psi|^2$ which vanishes at the vortex core; the squares denote the regions that are zoomed-in, on the bottom panels. The middle panels show the corresponding vector field $\mathbf{v}(\mathbf{x})$. The color map shows the amplitude of the current $\mathbf{j} = |\psi|\mathbf{v}$, while the arrows show the superflow vector field $\mathbf{v}(\mathbf{x})$. The bottom row shows the corresponding data zoomed closer to the various fixed points of $\mathbf{v}(\mathbf{x})$. The green and magenta circles highlight the vortices and saddle points of $\mathbf{v}(\mathbf{x})$ respectively, corresponding to different trajectories Γ in (3). The regime $l_z = 0.8$ features a single eccentric vortex as the unique fixed point of $\mathbf{v}(\mathbf{x})$. When $l_z = 1.4$, a second vortex together with a saddle point enters the condensate. Next, when $l_z = 2$, a third vortex enters the condensate, and it is accompanied with an additional saddle point of $\mathbf{v}(\mathbf{x})$. Finally, for $l_z = 2.5$ the third vortex has entered closer to the center of the condensate, to form a symmetric triangle. This is accompanied by a merging of the two saddle points into a saddle point with index $i_{\mathbf{v}} = -2$. Both the vortices and the saddle points are characterized by a vanishing superflow $|\mathbf{j}(\mathbf{x})| = 0$. Unlike the vortex cores, where the density $|\psi|$ vanishes, at the saddle points $|\psi| \neq 0$. This can be seen by comparing the data for the current $\mathbf{j} := |\psi|\mathbf{v}$, with the density $|\psi|^2$ data. Note that the saddle points can be interpreted as points where the superflows of different vortices cancel each other.

The Figure 2 shows examples of vortices and saddle points for different values of the macroscopic angular momentum l_z. The corresponding solutions of Eq. (5), describe how these structures rotate uniformly around the symmetry axis, with constant angular velocity $-\lambda_z^{min}$; see Eq. (13).

For $0 < l_z < 1$ the condensate features a unique vortex that is located off the trap center. Next, when $l_z = 1.4$, the minimal energy wave function features two additional fixed points of $\mathbf{v}(\mathbf{x})$, a vortex and a saddle point. Upon increasing l_z, the second vortex together with the saddle point move toward the trap center, until they form a symmetric pair of vortices with a saddle point in between (not shown). With a further increase of l_z, a third vortex and a second saddle point of $\mathbf{v}$ now appear, as can be seen when $l_z = 2.0$. Finally, for $l_z = 2.5$ the third vortex enters closer to the center of the condensate, to form a symmetric triangle. This is accompanied by a merging of the two saddle points into a higher degree fixed point; there is a degenerate saddle point with index $i_{\mathbf{v}} = -2$ at the center of the disk and it is surrounded by the three vortices.

The Figure 3 shows the evolution of the minimum energy state, when l_z is further increased. When $l_z = 3.8$, there are five single vortices, and a single saddle point with an index $i_{\mathbf{v}} = -4$. Next, when $l_z = 4.1$, the total number of vortices is now six. Three of the vortices are paired with a saddle point and the other three are individual. This implies according to the Poincaré index formula that the saddle point of the vector field $\mathbf{v}(\mathbf{x})$ at the center has index $i_{\mathbf{v}} = -4$.

The configuration for $l_z = 4.7$ in Fig. 3 consists of seven vortices, arranged in an almost triangular lattice. The central vortex here is isolated, while the six outer vortices

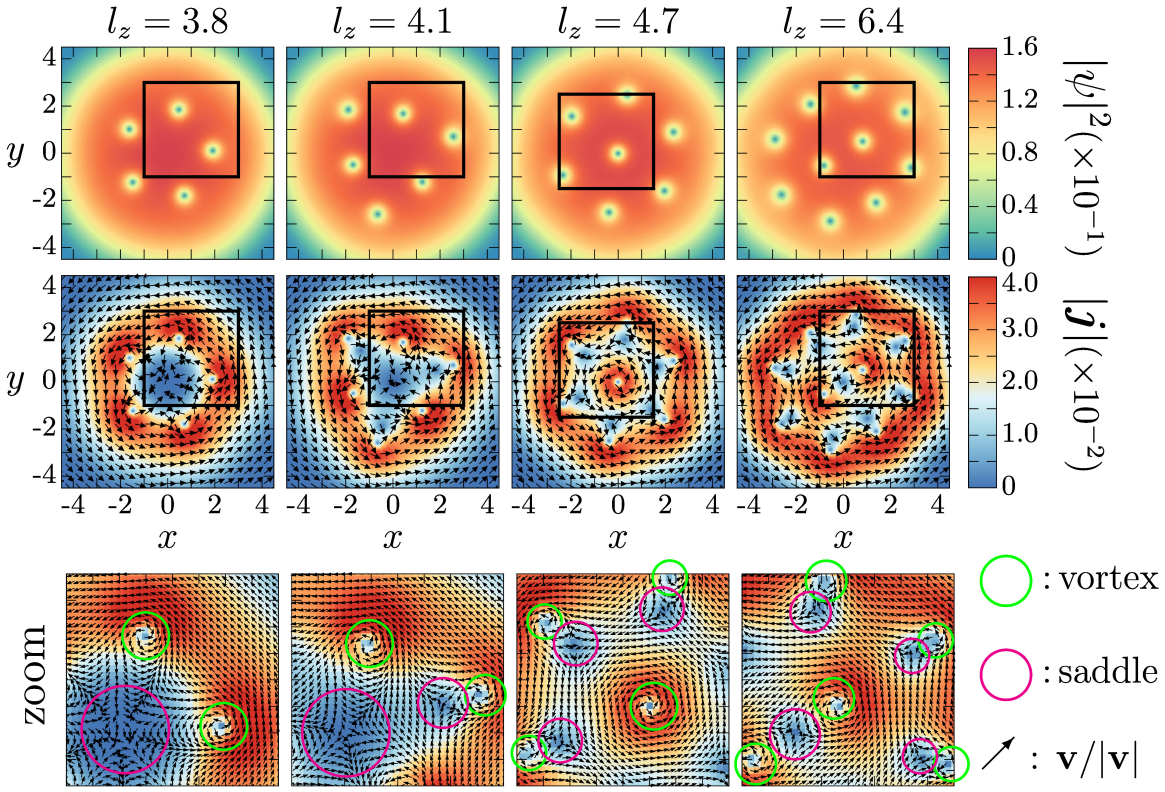

Figure 3. The panels show the minimal energy configurations for larger values of the angular momentum $L_z = l_z$ and $N = 1$ for the dimensionless coupling $g = 400$. The displayed quantities are the same as in Fig. 2. The regime $l_z = 3.8$ features five vortices accompanied by a unique saddle point of $\mathbf{v}(\mathbf{x})$ with Poincaré index $i_\mathbf{v} = -4$. When $l_z = 4.1$, a sixth vortex enters, and there three satellite saddle points with index $i_\mathbf{v} = -1$, and a single one with index $i_\mathbf{v} = -2$. Next, when $l_z = 4.7$, there are seven vortices with almost triangular lattice. Each of the six outer vortices here is paired with an simple saddle point. Finally, for $l_z = 6.4$ there are ten vortices and nine saddle points with index $i_\mathbf{v} = -1$.

with $i_\mathbf{v} = 1$ are tightly bound to six saddle-points with $i_\mathbf{v} = -1$. Finally the configuration with $l_z = 6.4$ consists in a pair of vortices bound to a central saddle-point, the whole being surrounded by eight bound pairs of vortex and saddle-points. This again satisfies the Poincaré index formula.

When the value of l_z is further increased, we observe that the patterns identified in Figures 2 and 3 are repeated: The difference between the vortices and saddle points is always one; when l_z increases the new vortices and saddle-points enter the disk together, as tightly bound pairs. The saddle points can either remain bound to the vicinity of the vortices. Alternatively, they can also proceed all the way to the disk center where they can either form condensed higher degree saddle points, or structures that are akin Abrikosov lattices. But the vortices always remain isolated and arrange themselves into co-centric Abrikosov lattices.

Finally, the figure 4 summarizes the main features that can be observed for the vector field $\mathbf{w}(\mathbf{x})$ (4), that is associated with density gradients.

SUMMARY

We have used the Poincaré index formula, in combination with numerical simulations to study the local topology and geometry of the two dimensional Gross-Pitaevskii equation, that models the ground state of a cold atom Bose-Einstein condensate in an axially symmetric disk-like, non-rotating harmonic trap. We have varied the angular momentum that is supported by the ground state wave function, and we have confirmed that the difference in the number of vortices and in the number of saddle points is always equal to one. In particular we have observed how the vortices and saddle points enter the condensate, always in pairs, when the angular momentum increases. We have observed how the vortices repel each other to form co-centric Abrikosov lattices, while the saddle points can either aggregate into higher degree fixed points or pair up with vortex cores as the angular momentum increases; the ensuing structures rotate around the trap center at constant angular velocity.

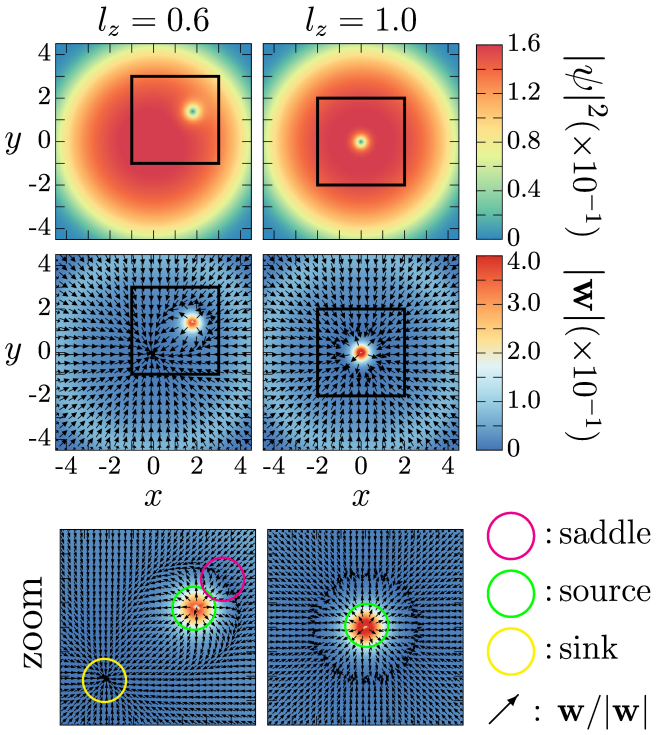

Figure 4. The panels show the minimal energy configurations for values of the angular momentum $l_z = 0.6$ and 1 and $N = 1$ for the dimensionless coupling $g = 400$. The panels on the top row display the density $|\psi|^2$. The middle panels display the corresponding vector field $\mathbf{w}(\mathbf{x})$, and the bottom line shows the corresponding data zoomed closer to the fixed points of $\mathbf{w}(\mathbf{x})$. The green and yellow circles respectively highlight the source (the vortex) and sink of $\mathbf{w}(\mathbf{x})$. The saddle point of $\mathbf{w}(\mathbf{x})$ is represented by magenta circle. All these circles correspond to different trajectories Γ in (3), for the vector field $\mathbf{w}(\mathbf{x})$. The configuration $l_z = 0.6$, features a single eccentric vortex (the source), and a sink of $\mathbf{w}(\mathbf{x})$. The index theorem dictates that there is also a saddle point. In the case where $l_z = 1$, there is a nodal line encircling the source. This is a degeneracy circle with index $i_{\mathbf{w}} = -1$ [12].

ACKNOWLEDGMENTS

This work is supported by the Swedish Research Council under Contract No. 2018-04411. The research by AJN is partially supported by the Carl Trygger Foundation Grant CTS 18:276 and by Grant No. 0657-2020-0015 of the Ministry of Science and Higher Education of Russia. AJN also acknowledges collaboration under COST Action CA17139. The computations were performed on resources provided by the Swedish National Infrastructure for Computing (SNIC) at National Supercomputer Center at Linköping, Sweden.

* garaud.phys@gmail.com
† Antti.Niemi@su.se

[1] M. Nakahara, *Geometry, Topology and Physics* (CRC Press, 2003).
[2] M. H. Anderson, J. R. Ensher, M. R. Matthews, C. E. Wieman, and E. A. Cornell, "Observation of Bose-Einstein Condensation in a Dilute Atomic Vapor," Science **269**, 198–201 (1995).
[3] K. B. Davis, M.-O. Mewes, M. R. Andrews, N. J. van Druten, D. S. Durfee, D. M. Kurn, and W. Ketterle, "Bose-Einstein Condensation in a Gas of Sodium Atoms," Physical Review Letters **75**, 3969–3973 (1995).
[4] C. C. Bradley, C. A. Sackett, and R. G. Hulet, "Bose-Einstein Condensation of Lithium: Observation of Limited Condensate Number," Physical Review Letters **78**, 985–989 (1997).
[5] D. C. Aveline, J. R. Williams, E. R. Elliott, C. Dutenhoffer, J. R. Kellogg, J. M. Kohel, N. E. Lay, K. Oudrhiri, R. F. Shotwell, N. Yu, and R. J. Thompson, "Observation of Bose–Einstein condensates in an Earth-orbiting research lab," Nature **582**, 193–197 (2020).
[6] E. R. Elliott, M. C. Krutzik, J. R. Williams, R. J. Thompson, and D. C. Aveline, "NASA's Cold Atom Lab (CAL): system development and ground test status," npj Microgravity **4**, 16 (2018).
[7] I. Bloch, J. Dalibard, and S. Nascimbène, "Quantum simulations with ultracold quantum gases," Nature Physics **8**, 267–276 (2012).
[8] E. B. Sonin, *Dynamics of Quantised Vortices in Superfluids* (Cambridge University Press, Cambridge, 2016).
[9] P. Hartman, *Ordinary Differential Equations* (John Wiley & Sons, New York, 1964).

[10] J. Llibre and J. Villadelprat, "A Poincaré index formula for surfaces with boundary," Differential Integral Equations **11**, 191–199 (1998).
[11] N. Lloyd, *Degree theory* (Cambridge University Press, Cambridge New York, 1978).
[12] H. Ruan and J. Zanelli, "Degeneracy Index and Poincaré-Hopf Theorem," (2019), arXiv:1907.01473 [math-ph].
[13] W. Bao and Y. Cai, "Mathematical theory and numerical methods for Bose-Einstein condensation," Kinetic & Related Models **6**, 1–135 (2013).
[14] J. Garaud, J. Dai, and A. J. Niemi, "Vortex precession and exchange in a Bose-Einstein condensate," Journal of High Energy Physics **2021**, 157 (2021).
[15] F. Wilczek, "Quantum Time Crystals," Physical Review Letters **109**, 160401 (2012).
[16] A. Alekseev, J. Dai, and A. J. Niemi, "Provenance of classical Hamiltonian time crystals," Journal of High Energy Physics **2020**, 35 (2020).
[17] J. E. Marsden and T. S. Ratiu, *Introduction to Mechanics and Symmetry* (Springer New York, New York, 1999).
[18] F. Hecht, "New development in freefem++," Journal of Numerical Mathematics **20**, 251–265 (2012), See also FreeFEM software at `https://freefem.org/`.